Origins of biweekly sea surface temperature variability in the eastern equatorial Pacific and Atlantic

Gaopeng Xu[1], Ping Chang[1,2], and Qiuying Zhang[1]

[1]Department of Oceanography, Texas A&M University, College Station, Texas, USA

[2]Department of Atmospheric Sciences, Texas A&M University, College Station, Texas, USA

Corresponding author: Gaopeng Xu (gaopxu@tamu.edu); Qiuying Zhang (zhangqiuying@tamu.edu)

Abstract

Biweekly sea surface temperature (SST) variability significantly contributes to over 50% of the intraseasonal variability in the eastern equatorial Pacific (EEP) and Atlantic (EEA). Our study investigates this biweekly variability, employing a blend of in-situ and reanalysis datasets. The research identifies biweekly signals in SST, meridional wind, and ocean currents, notably in September-November in EEP and June-August in EEA. Biweekly southerly (northerly) drives simultaneous northward (southward) ocean currents in EEP, but with a 1-2-day phase delay in EEA. Consequently, these currents lead to SST anomalies with a 3-4-day lag in both EEP and EEA due to the presence of the cold tongue. The study reveals the origin of biweekly wind fluctuations in the western Pacific for EEP and the subpolar Pacific for EEA, connected by Rossby waves validated through a linearized non-divergent barotropic model. This research affirms the influence of subtropical and subpolar atmospheric forcing on equatorial SST.

Key points

- Over 50% of intraseasonal SST variability in the eastern equatorial Pacific and Atlantic is attributed to biweekly fluctuations.
- The atmospheric winds play a crucial role in driving the biweekly SST variability.
- Biweekly winds associated with biweekly SST variability in the equatorial regions stem from both the subtropical and subpolar regions.

Plain language summary

Our research focuses on understanding the regular changes in sea surface temperature (SST) occurring every two weeks, which significantly contribute to the seasonal variations in the eastern equatorial Pacific (EEP) and Atlantic (EEA). By analyzing a mix of direct and reconstructed data, we uncover the distinct patterns of these biweekly changes in SST, winds, and ocean currents. Our investigation shows that the movements of the ocean currents are closely linked to the shifts in wind direction, affecting the temperature of the ocean waters. Notably, we observe a delay in the relationship between wind and SST in both EEP and EEA. Through our analysis, we establish that the origins of these biweekly wind patterns can be traced to specific regions in the Pacific. Moreover, we identify the role of Rossby waves in connecting these wind patterns to their source regions, which helps us understand how changes in atmospheric conditions in different parts of the ocean can impact the equatorial SST.

1. Introduction

Intraseasonal variability (ISV) encompasses phenomena characterized by periods shorter than 90 days, primarily manifesting in equatorial oceans. It includes equatorial Kelvin waves with a period of 60-75 days (Kessler et al., 1995; McPhaden & Taft, 1988), Madden-Julian Oscillation with a period of 30-60 days which can influence sea surface temperature (SST) through surface fluxes (Han et al., 2007; Lau & Waliser, 2011; Madden & Julian, 1971; Shinoda et al., 1998), tropical instability waves (TIWs) with a period of 20-40 days (Chelton et al., 2000, 2001; Düing et al., 1975; Legeckis, 1977; Lyman et al., 2007), and variability occurring every 10 to 20 days, often referred to as biweekly variability (Athie & Marin, 2008; Diakhaté et al., 2016; Han et al., 2006).

MJO exerts its strongest influence over the Indian Ocean and Western Pacific regions, but TIWs are generally observed in the eastern Pacific and western Atlantic. Kelvin waves are often triggered by wind anomalies (Hendon et al., 1998; Kessler et al., 1995) while the generation of TIWs is attributed to the instability of the equatorial currents (Cox, 1980; Flament et al., 1996; Jochum et al., 2004; Luther & Johnson, 1990; Masina et al., 1999; Philander, 1976, 1978; Proehl, 1996; Von Schuckmann et al., 2008; Yu & Liu, 2003). Notably, the biweekly variability, although less studied than other intraseasonal variabilities, has been observed in the eastern equatorial Atlantic (EEA) (Athie & Marin, 2008; Coëtlogon et al., 2010; Houghton & Colin, 1987), but, to the best of our knowledge, has yet to be comprehensively investigated in the eastern equatorial Pacific (EEP).

The study of biweekly SST variability in the EEA dates back to the 1980s, with Houghton and Colin (1987) identifying a prominent peak every 15 days in the cospectrum of ocean currents and temperatures near the equator at 4°W. Athie and Marin (2008) conducted a comprehensive analysis, revealing a distribution pattern east of 10°W during boreal summer, without significant zonal propagation features. They suggested that the biweekly SST signal is passively driven by meridional winds and influenced by the cold tongue front, corroborated by Jouanno et al. (2013). In contrast, de Coëtlogon et al. (2010) proposed a robust negative feedback mechanism between SST and surface winds in the Gulf of Guinea during boreal spring and summer. They argued that intensified southerly winds, which may be associated with the St. Helena anticyclone (Banzon et al., 2016; Reynolds et al., 2007), lead to a cold SST anomaly within 5 days, subsequently slowing down the surface wind within 2-3 days, thereby maintaining biweekly variability. Other studies (de Coëtlogon et al., 2014; Leduc-Leballeur et al., 2013) also supported this negative feedback mechanism, highlighting the influence of biweekly SST on the pressure gradient in the atmospheric boundary layer in the EEA.

Given the unclear source of biweekly wind signals, this study will delve deeper into the origins of these biweekly wind patterns. Additionally, we will examine and compare the generation mechanism driving biweekly SST variability in EEP and EEA. The subsequent sections of this paper will provide a detailed description of the data and methodologies (Section 2), followed by spatial and temporal analyses of biweekly variability in EEP and EEA (Section 3). Relationships among biweekly SST, surface wind, and ocean currents in both regions will be explored in Section 4. Section 5 will focus on deciphering the origins of biweekly atmospheric variabilities associated with SST. Finally, Section 6 will offer conclusions and discussions.

2. Data and methods

2.1. Data

The study relies on reanalysis datasets from 1994 to 2014. The daily SST data with a spatial resolution of 1/4° are sourced from the NOAA Optimum Interpolation SST (OISST) version 2, derived from the satellite data and ship observations (Reynolds et al., 2007). Two different daily wind datasets are utilized in our analysis. One is the Cross-Calibrated Multi-Platform (CCMP) version 3.0 dataset with a horizontal resolution of 1/4° (Atlas et al., 2011). The other is from the ECMWF global reanalysis product known as ERA-interim providing wind vectors up to 0.1 hPa with horizontal resolution of 80 km (Berrisford et al., 2009; Dee et al., 2011).

Surface oceanic currents are taken from HYCOM reanalysis 3.1 with horizontal resolution of 1/12° (Cummings, 2005; Cummings & Smedstad, 2013). Moreover, we incorporate SST data from two equatorial mooring arrays. One is situated at (95°W, 0°N) as part of the Tropical Atmosphere Ocean (TAO) project (McPhaden et al., 1998) while the other is located at (0°W,0°N) within the Prediction and Research Moored Array in the Tropical Atlantic (PIRATA) network (Bourlès et al., 2008).

2.2. Methods

Wavelet analysis (Torrence & Compo, 1998) is utilized in this study to extract frequency-related information from SST, meridional wind, and meridional ocean velocity time series after applying the Hann filter to reduce spectral leakage. Monthly climatology of wavelet spectrum is employed to illustrate biweekly oscillations.

Singular value decomposition (SVD) is generally used to study covarying patterns of two interrelated variables (Bretherton et al., 1992). It will be empirical orthogonal function (EOF) analysis when two variables are the same. Prior to the decomposition process, a 10-20-day bandpass filter is applied to each variable. The leading SVD mode (SVD1) typically accounts for the most significant covariance between two variables. By performing SVD on two variables with time lags, we can explore the temporal relationship between the two variables, providing insights into potential causality among SST, surface wind and oceanic currents.

3. Spatial and temporal characteristics of biweekly variability

Figure 1a shows the ratio between the standard deviation of 10-20-day bandpass filtered SST and that of 90-day high-pass filtered SST, with a focus on ratios exceeding 0.5. Notably, the respective largest ratio is in proximity to the coordinates (95°W,0°N) in EEP and (0°W,0°N) in EEA, implying the predominance of biweekly SST variability within the spectrum of intraseasonal variability. In the equatorial Pacific, the strong biweekly SST variability extends from 100°W to 90°W, which is distinct from TIWs' region spanning from 110°W to 160°W (Chelton et al., 2000). In alignment with the findings of Athie and Marie (2008), the equatorial Atlantic shows strong biweekly SST variability within the range of 10°W-5°E, which is also different from the TIWs' region. It is noteworthy that both regions fall within the cold tongue zone of their respective oceans.

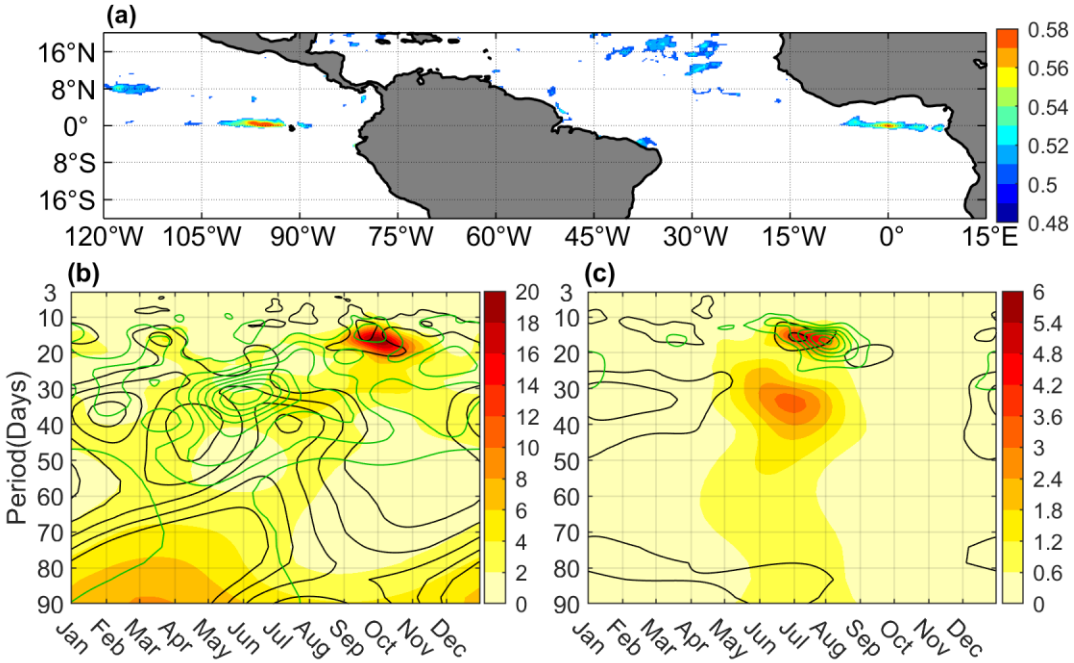

Figure 1 **(a)** Ratio of 10-20-day high-pass filtered SST standard deviation to that of 90-day high-pass filtered SST (OISST) from 1994 to 2014, displayed for values larger than 0.5; **(b)** monthly climatology of wavelet spectrum of SST from TAO (color), meridional wind from CCMP (black contour) and meridional ocean current from HYCOM (green contour) at (95°W,0°N) in 1996, 2000, 2002, 2003, 2005, 2006, 2011; **(c)** monthly climatology of wavelet spectrum of SST (color) and meridional wind (black contour) from CCMP at (0°W,0°N) in 2003, 2006, 2011, 2012, 2016, 2017, 2018 and meridional ocean current from HYCOM (green contour) at (0°W,0°N) in 2003, 2006, 2011, 2012. Black contours start from 0 to 5 with interval as 1, green contours start from 0 to 0.4 with interval as 0.04.

Within the regions exhibiting strong biweekly signals, we have access to valuable temporal data from two moored buoys for closer examination. One buoy is positioned at (95°W,0°N) from TAO, while the other is situated at (0°W,0°N) from PIRATA. To ensure consistency in our analysis, we have meticulously chosen seven complete years at each location for evaluation. These years include 1996, 2000, 2002, 2003, 2005, 2006, 2011 at (95°W,0°N) and 2003, 2006, 2011, 2012, 2016, 2017, 2018 at (0°W,0°N). Unfortunately, the corresponding surface wind and ocean current measurements have too many missed values. Therefore, we rely on surface wind data from CCMP and ocean current data from HYCOM for our analysis. Since HYCOM data is only available up to 2015, only 4 years (2003, 2006, 2011, 2012) of ocean current data are used in the analysis at (0°W,0°N). Before conducting the wavelet analysis, we concatenate all the time series data and eliminate the seasonal cycle to ensure robust and consistent results.

Figure 1b and 1c present the monthly climatology of wavelet energy spectrums for SST (shading), meridional wind (black contour) and meridional ocean current (green contour) at (95°W,0°N) and (0°W,0°N), respectively. In the case of SST, the spectrum reveals a prominent energy peak occurring between 10-20 days from September to November at (95°W,0°N).

Similarly, meridional wind and ocean current exhibit local energy peaks during these months, as well as from February to April. We also note that 30-50-day meridional wind variability is more dominant and persists for a longer duration, but there is no strong SST variability in this frequency band that corresponds to the wind variability. As shown in Figure 1c, all three variables exhibit energy peaks during June-August at (0°W,0°N), with meridional wind and ocean velocity also showing a minor peak in March, which aligns with the findings of Diakhaté et al. (2016).

Two notable distinctions in biweekly SST variability between the Pacific and Atlantic regions emerge. Firstly, the timing of occurrence appears to be linked to the development of the cold tongue phenomenon, which is well-established during the boreal fall in the Pacific (Wyrtki, 1981) and in the boreal summer in the Atlantic (Xie & Carton, 2004). Secondly, there is a disparity in amplitude, with the Pacific exhibiting higher SST variance, potentially reaching up to 18, compared to the Atlantic's variance, which typically reaches around 5. It's important to emphasize that this study's primary focus is on understanding the generation mechanisms of biweekly variabilities, rather than the amplitude disparities. For the forthcoming analysis, we will utilize data spanning from May to August in the Atlantic and from August to November in the Pacific. This choice allows us to commence our analysis from the month before biweekly variability becomes fully developed in each respective region. Additionally, given that OISST can replicate buoy SST spectral characteristics (Figure S1), we will employ OISST data in our subsequent analyses.

4. Relationships between SST, surface wind and ocean currents

Figure 2a and 2e show the results of coherence between 90-day high-pass filtered SST and meridional wind at (95°W,0°N) and (0°W,0°N), respectively. Evidently, coherence values peak within the 10- and 20-day range in both the Pacific and Atlantic regions. The corresponding phase between SST and wind hovers around -50^{o}, indicating that SST leads wind by approximately 2 days or, conversely, wind leads SST by roughly 5 days.

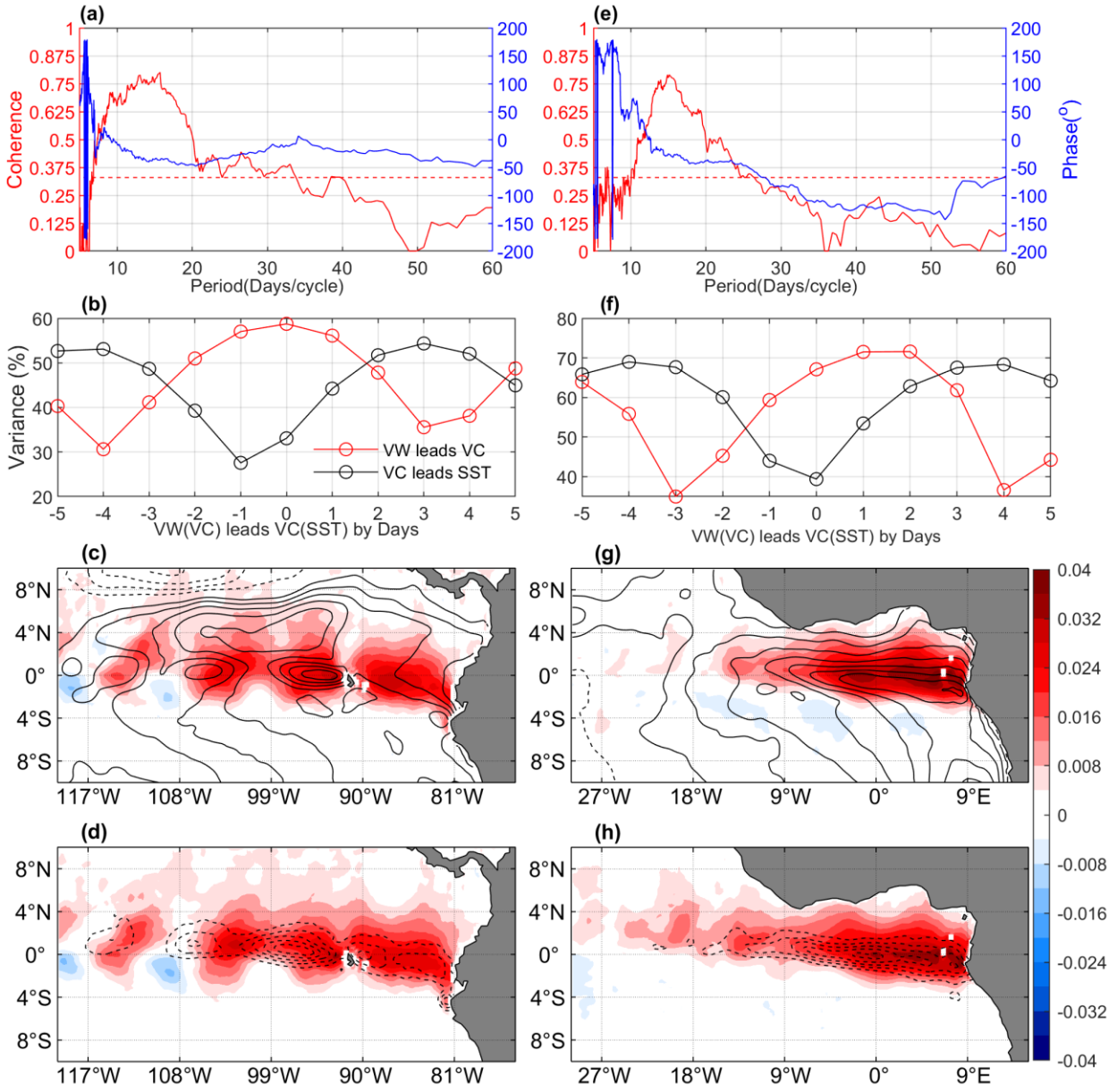

Figure 2 Coherence (red) and phase (blue) between SST (OISST) and meridional wind (CCMP) at (95°W, 0°N) in the Pacific **(a)** and at (0°W, 0°N) in the Atlantic **(e)** with a dashed red line indicating the 99% significance level. Negative phase represents SST leads wind speed. Explained variance by SVD1 for meridional wind (VW) and ocean current (VC, red), and SST and VC (black) is presented for different lead-lag times in the Pacific **(b)** and Atlantic **(f)**. **(c)** SVD1 of VW (contour) and VC (shading) with zero lag in the Pacific; **(d)** SVD1 of SST (contour) and VC (shading) with VC leading SST by 3 days in the Pacific; **(g)** similar to (b), but with VW leading VC by 2 days in the Atlantic; **(h)** similar to (d), but with VC leading SST by 4 days in the Atlantic. Dashed (solid) contours represent negative (positive) value. Contours start from -0.05 to 0.05 with interval 0.002 for VW and 0.01 for SST. All data used here are from August to November in the Pacific and from May to August in the Pacific in 1994-2014.

To verify the relationships between SST, meridional wind and ocean current, we conducted a lagged SVD analysis. Figure 2b illustrates the explained covariance by SVD1 at various time lags in the Pacific. It is evident that the explained covariance between meridional wind and current reaches the maximum (58.76%) at lag=0. The explained covariance by ocean current and SST reaches maximum (54.36%) when ocean current leads SST by 3 days.

The simultaneous SVD1 of biweekly meridional wind and ocean current is shown in Figure 2c. Both biweekly wind and ocean current exhibit a wave-like structure along the equator. It's important to note that the Wheeler-Kiladis dispersion relation analysis, although not shown here, does not reveal any distinct propagating waves. Despite the biweekly wind (black contour) demonstrating a broader spatial pattern compared to the ocean current (color shading), the overall consistency in structures of these two confirms that the northward wind leads to northward current. In Figure 2d, the spatial patterns of SVD1 with the meridional ocean current (color shading) leading SST (black contour) by 3 days highlight northward ocean currents can result in SST cooling.

In the Atlantic, the maximum of the explained covariance (Figure 2f) occurs when wind leads ocean current by 1 or 2 days (71.59%) and ocean currents then leads SST by 3 or 4 days (68.34%). Spatial patterns of SVD1 with the highest explained covariance in the Atlantic (Figure 2g&2h) are similar to those in the Pacific. The structures of biweekly SST exhibit asymmetry across the equator in both the Pacific and Atlantic. This asymmetry is likely a result of the positioning of SST fronts in the Pacific and Atlantic (De Szoeke et al., 2007; Giordani & Caniaux, 2014), which agrees with the argument by Athie and Marie (2008) that SST front can modulate biweekly SST variability. In summary, the SVD analysis suggests that biweekly meridional wind drives variability in meridional ocean current. Consequently, the northward (southward) ocean current transports cold (warm) water northward (southward), contributing to the generation of biweekly SST variability.

5. Origins of biweekly wind variability

To examine the dominant mode of biweekly winds, we present EOF1 and PC1 of 10–20-day wind vector during August-November in the Pacific and during May-August in the Atlantic in Figure S2. The expansive structure of the wind extends to at least 20°S in both the Pacific and Atlantic (Figure S2b&d), suggesting a potential linkage between the equatorial winds and subtropical winds. Patricola and Chang (2017) and Risien et al. (2004) also found biweekly variability of wind along the Africa coast near 20^{o}S in the Atlantic. This raises the possibility that the equatorial biweekly variability may be associated with atmospheric processes in the subtropical regions. de Coëtlogon et al. (2010) and Patricola and Chang (2017) highlighted that biweekly wind variabilities in the equatorial or Benguela regions are closely related to the St Helena high. The wind vectors in Figure S2b&d demonstrate a coherent large-scale atmospheric circulation pattern, indicating a connection between wind variability in the subtropics and equatorial regions in both the Pacific and Atlantic.

To ascertain the origins of the biweekly wind signals in the eastern Pacific, we conducted a regression analysis of the 90-day high-pass filtered wind at 500hPa during August-November onto PC1 of the surface wind (Figure S2a) at various time lags of 0, 2, 4, and 6 days (Figure 3a-d). The results reveal a distinct eastward propagation of a biweekly wave train from the east of Australia to the South America, with a zonal wavelength of approximately 6,000 km. This wave train bears a close resemblance to similar findings reported by Ambrizzi et al. (1995). Moreover,

Li et al. (2015) demonstrated that the western Pacific region around 20°S-40°S serves as a significant Rossby wave source, influenced by the strong jet and the descending branch of the Hadley Cell. Shimizu and de Albuquerque Cavalcanti (2011) also identified the Western Pacific (160°E-160°W, 10°S-30°S) as a significant Rossby wave source. Therefore, we hypothesize that the biweekly wave train depicted in Figure 3a-d originates from the western South Pacific around 30ºS with a slight southward propagation and finally is trapped between 30ºS and 45ºS. The wave patterns not only manifest at 500hPa but also extend up to 300hPa (Figure S3a-d), suggesting the Rossby waves exhibit barotropic structures.

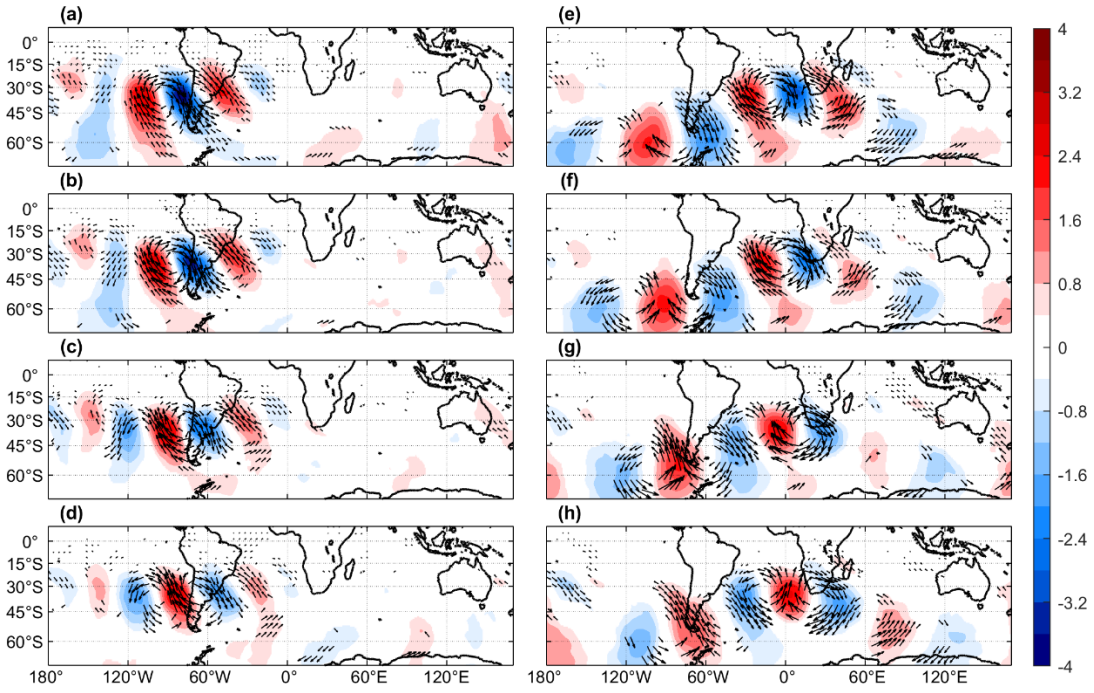

Figure 3 **(a)-(d)** Regression coefficient of 90-days high-passed wind at 500hPa in August-November onto the PC1 in Figure S2a with lagged time of 0, 2, 4, 6 days; **(e)-(h)** similar to (a)-(d) but in May-August onto the PC1 in Figure S2c. Shading represents regression coefficients of meridional wind.

Figure 3e-h illustrates the regression coefficient of 90-day high-passed wind at 500hPa during May-August onto the PC1 of the surface wind in the Atlantic (Figure S2b). The resulting biweekly wave train exhibits a trajectory extending to the subpolar South Pacific with a zonal wavelength of approximately 9,000 km and meridional wavelength of 2,000 km. In accordance with Shimizu and de Albequerque Cavalcanti (2011), the region south of Australia is recognized as another significant Rossby wave source. Therefore, we postulate that the origin of the biweekly wave train may be attributed to the Rossby wave source situated south of Australia. To further substantiate our hypotheses, we will analyze biweekly wave energy propagation according to Rossby wave ray theory (Hoskins & Ambrizzi, 1993; Hoskins & Karoly, 1981; Karoly, 1983).

As shown in Figure 3a-d, the biweekly wave trains in the Pacific are trapped in the subtropics, with a zonal wavelength (wavenumber) of trapped waves is approximately 6,000 km (1.01×10^{-6}

rad/m). Based on the linearized vorticity equation, the necessary condition for trapped Rossby waves can be expressed as $\Delta = \beta_M k/(kU-\omega) - k^2 < 0$, where U represents the zonal mean velocity from 180°E to 120°W (Figure S4), $\beta_M = \beta - U_{yy}$ is the meridional gradient of absolute vorticity, ω is the frequency, and k is the zonal wavenumber. By considering $k = 1.01 \times 10^{-6}\, rad/m$, the variation of Δ with latitude for $\omega = 2\pi/10days$ and $2\pi/20days$ is presented in Figure 4a. The results suggest that biweekly Rossby waves with a small meridional wavenumber are likely to be trapped between 35°S and 55°S.

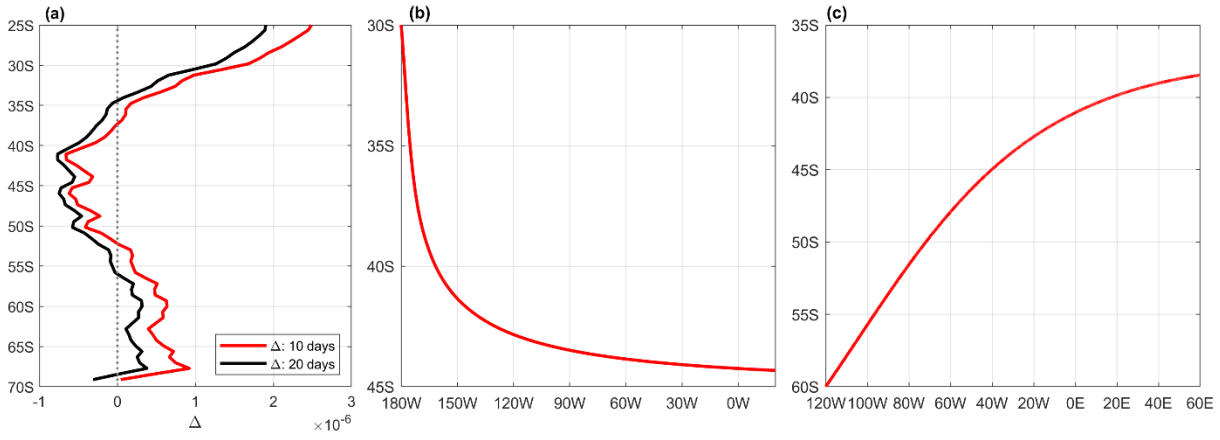

Figure 4 **(a)** Necessary conditions as function of latitude with frequency as $2\pi/10days$ (red) and $2\pi/20days$ (black) for the Pacific case, where zonal velocity is taken as the climatology of zonal mean between 180°W and 120°W from ERA-Interim; **(b)** Trajectory of Rossby waves from linearized barotropic non-divergent model for the Pacific case. **(c)** similar to (b), but for the Atlantic case.

Ray theory provides an additional approach for verifying the trace of Rossby waves (Huskins and Karoly, 1981). The trajectory of Rossby waves can be derived from the dispersion relation as follows:

$$\frac{dk}{dt} = -\frac{\partial \omega}{\partial x} = 0, \frac{dl}{dt} = -\frac{\partial \omega}{\partial y} = -U_y k + \frac{\beta_M y k}{k^2+l^2}, \frac{dx}{dt} = \frac{\partial \omega}{\partial k} = \frac{\omega}{k} + \frac{2\beta_M k^2}{(k^2+l^2)^2}, \frac{dy}{dt} = \frac{\partial \omega}{\partial l} = \frac{2\beta_M kl}{(k^2+l^2)^2},$$

where l is the meridional wavenumber decaying rapidly with the increase of $|y|$. The ray for biweekly Rossby waves with $k = 1.01 \times 10^{-6}\, rad/m$ (Figure 4b) suggests that the waves generated at 30°S will propagate poleward and eventually be trapped between 30°S and 45°S. The coherence between the observations and theoretical results provides evidence supporting the likelihood that biweekly variability in the eastern Pacific originates from western Pacific.

As indicated in Figure 3e-h, the waves related to the biweekly signals in the Atlantic propagate northeastward from the subpolar Pacific to the subtropical Atlantic. This trajectory differs from the one associated with biweekly variability in EEP that shows no northward propagation. The ratio of meridional wind velocity to zonal wind velocity reaches 0.4 in the subpolar Pacific (Figure S5), emphasizing the significance of meridional velocity in modulating Rossby waves in this region. Therefore, meridional velocity is considered in the reproduction of wave rays using the barotropic nondivergent model proposed in Karoly (1982): $\left(\frac{\partial}{\partial t} + U\frac{\partial}{\partial x} + V\frac{\partial}{\partial y}\right)\left(\frac{\partial^2 \psi}{\partial x^2} + \frac{\partial^2 \psi}{\partial y^2}\right) +$

$q_y \frac{\partial \psi}{\partial x} + q_x \frac{\partial \psi}{\partial y} = 0$, where $q = \frac{\partial^2 \psi}{\partial x^2} + \frac{\partial^2 \psi}{\partial y^2} + f$ and f is Coriolis parameter, U is taken as constant, and V is meridional velocity as a function of latitude. The wave solution, with the form of $\psi = A(X,Y,T)e^{i(kx+ly-\omega t)}$, yields the dispersion relation : $\omega = Uk + Vl + \left(q_x l - q_y k\right)/(k^2 + l^2)$. Based on the conservations of crests and the definition of group velocity, the equations governing wave rays can be expressed as $\frac{d_g k}{dt} = -\frac{\partial \omega}{\partial x} = 0$, $\frac{d_g l}{dt} = -\frac{\partial \omega}{\partial y} = -U_y k - V_y l + \frac{q_{yy} k - q_{xy} l}{k^2 + l^2}$, $\frac{dx}{dt} = \frac{\partial \omega}{\partial k} = U + \frac{(k^2 - l^2) q_y - 2kl q_x}{(k^2 + l^2)^2}$, $\frac{dy}{dt} = \frac{\partial \omega}{\partial l} = V + \frac{2kl q_y + (k^2 - l^2) q_x}{(k^2 + l^2)^2}$. Consequently, when the meridional velocity V and $\left[2kl q_y + (k^2 - l^2) q_x\right]/(k^2 + l^2)^2$ are balanced, the waves will be trapped within a specific latitude band. Considering U as 15 m/s and V gradually decreasing from 6 m/s to 0 m/s toward the equator, the Rossby waves show northeastward propagation and eventually become trapped between 30°S and 45°S (Figure 4c). The agreement between the trajectories obtained by ray theory and the lag regression indicates that the Rossby waves associated with the biweekly wind variability in the Atlantic can be traced back to their origin in the Pacific.

6. Conclusion and discussion

In this study, we investigate biweekly variabilities in EEP and EEA using the buoy and reanalysis datasets from 1994 to 2014. Our findings suggest that biweekly SST variability can account for more than 50% intraseasonal variability. Wavelet analyses of SST, meridional wind and ocean current corroborate the prevalence of strong biweekly fluctuations, primarily occurring between September and November in EEP and between June and August in EEA. Coherence analysis and lead-lag SVD analyses both indicate that biweekly SST variability is primarily driven by the atmosphere forces with ocean currents acting as intermediaries. Biweekly meridional ocean currents are propelled by wind forcing, with a lag of 1-2 days in EEA but occurring simultaneously in EEP. Subsequently, ocean currents transport cold (warm) water northward (southward), resulting in the development of cold (warm) SST anomalies along the equator in 3-4 days.

Several studies (Garzoli, 1987; Houghton & Colin, 1987; Jouanno et al., 2013) suggested that biweekly ocean current variability in the eastern Atlantic is mixed Rossby-gravity wave following a dispersion relation of $k = \omega/c - \beta/\omega$. If c is taken as first baroclinic gravity wave speed 2.3 m/s, biweekly waves should have a corresponding wavelength 2300 km. However, our SVD analyses and the conclusions of Athie and Marin (2008) do not support the presence of propagation features in biweekly variabilities, contrary to the expectations of mixed Rossby-gravity waves. Furthermore, the observations used in Houghton and Colin (1987) and Garzoli (1987) were from a single point, lacking necessary wavelength information. In addition, Athie and Marin (2008) suggested the impact of the cold tongue on biweekly SST variability, a proposition that aligns with the results in this study.

The biweekly wind shows a broader structure compared to SST and ocean currents, extending to at least 20°S, suggesting a potential connection between equatorial and subtropical winds. By employing lead-lag regression analysis and a linearized barotropic nondivergent model, we establish the origin of biweekly wind variability in the eastern Pacific as the western Pacific and in the eastern Atlantic as the subpolar Pacific. While biweekly Rossby waves might not directly propagate to the equatorial regions, they can still influence the EEP and EEA through the trade

winds (Figure S2b&c). However, it is important to note that our trajectory analyses rely on simplified meridional wind velocity representations, assuming zero values in the EEP analysis and an exponentially decaying function in the EEA analysis. To further validate biweekly Rossby wave generation, it would be beneficial to conduct experiments using comprehensive atmosphere models in the future.

Acknowledgement

G. Xu and Q. Zhang acknowledge the support from the China Scholarship Council. We thank TAMU Supercomputing Facility and the Texas Advanced Computing Center (TACC) for providing the computing resources for this research.

Open Research

OISST is available at Reynolds et al. (2007). CCMP wind vector product is available at Remote Sensing Systems (2022). EAR-Interim wind vector product is available at ECMWF (2019). HYCOM data is available at NRL (2017).

References

Ambrizzi, T., Hoskins, B. J., & Hsu, H.-H. (1995). Rossby wave propagation and teleconnection patterns in the austral winter. *Journal of Atmospheric Sciences*, *52*(21), 3661–3672.

Athie, G., & Marin, F. (2008). Cross-equatorial structure and temporal modulation of intraseasonal variability at the surface of the tropical Atlantic Ocean. *Journal of Geophysical Research: Oceans*, *113*(C8).

Atlas, R., Hoffman, R. N., Ardizzone, J., Leidner, S. M., Jusem, J. C., Smith, D. K., & Gombos, D. (2011). A cross-calibrated, multiplatform ocean surface wind velocity product for meteorological and oceanographic applications. *Bulletin of the American Meteorological Society*, *92*(2), 157–174.

Berrisford, P., Dee, D., Fielding, K., Fuentes, M., Kallberg, P., Kobayashi, S., & Uppala, S. (2009). The ERA-interim archive. *ERA Report Series*, (1), 1–16.

Bourlès, B., Lumpkin, R., McPhaden, M. J., Hernandez, F., Nobre, P., Campos, E., et al. (2008). The PIRATA program: History, accomplishments, and future directions. *Bulletin of the American Meteorological Society*, *89*(8), 1111–1126.

352 Bretherton, C. S., Smith, C., & Wallace, J. M. (1992). An intercomparison of methods for
353 finding coupled patterns in climate data. *Journal of Climate*, *5*(6), 541–560.
354 Chelton, D. B., Wentz, F. J., Gentemann, C. L., de Szoeke, R. A., & Schlax, M. G. (2000).
355 Satellite microwave SST observations of transequatorial tropical instability waves.
356 *Geophysical Research Letters*, *27*(9), 1239–1242.
357 Chelton, D. B., Esbensen, S. K., Schlax, M. G., Thum, N., Freilich, M. H., Wentz, F. J., et al.
358 (2001). Observations of coupling between surface wind stress and sea surface
359 temperature in the eastern tropical Pacific. *Journal of Climate*, *14*(7), 1479–1498.
360 Coëtlogon, G. de, Janicot, S., & Lazar, A. (2010). Intraseasonal variability of the ocean—
361 atmosphere coupling in the Gulf of Guinea during boreal spring and summer. *Quarterly*
362 *Journal of the Royal Meteorological Society*, *136*(S1), 426–441.
363 de Coëtlogon, G., Leduc-Leballeur, M., Meynadier, R., Bastin, S., Diakhaté, M., Eymard, L., et
364 al. (2014). Atmospheric response to sea-surface temperature in the eastern equatorial
365 Atlantic at quasi-biweekly time-scales. *Quarterly Journal of the Royal Meteorological*
366 *Society*, *140*(682), 1700–1714.
367 Cox, M. D. (1980). Generation and propagation of 30-day waves in a numerical model of the
368 Pacific. *Journal of Physical Oceanography*, *10*(8), 1168–1186.
369 Cummings, J. A. (2005). Operational multivariate ocean data assimilation. *Quarterly Journal of*
370 *the Royal Meteorological Society: A Journal of the Atmospheric Sciences, Applied*
371 *Meteorology and Physical Oceanography*, *131*(613), 3583–3604.
372 Cummings, J. A., & Smedstad, O. M. (2013). Variational data assimilation for the global ocean.
373 In *Data assimilation for atmospheric, oceanic and hydrologic applications (Vol. II)* (pp.
374 303–343). Springer.

De Szoeke, S. P., Xie, S.-P., Miyama, T., Richards, K. J., & Small, R. J. O. (2007). What maintains the SST front north of the eastern Pacific equatorial cold tongue? *Journal of Climate*, *20*(11), 2500–2514.

Dee, D. P., Uppala, S. M., Simmons, A. J., Berrisford, P., Poli, P., Kobayashi, S., et al. (2011). The ERA-Interim reanalysis: Configuration and performance of the data assimilation system. *Quarterly Journal of the Royal Meteorological Society*, *137*(656), 553–597.

Diakhaté, M., De Coëtlogon, G., Lazar, A., Wade, M., & Gaye, A. T. (2016). Intraseasonal variability of tropical Atlantic sea-surface temperature: air–sea interaction over upwelling fronts. *Quarterly Journal of the Royal Meteorological Society*, *142*(694), 372–386.

Düing, W., Hisard, P., Katz, E., Meincke, J., Miller, L., Moroshkin, K., et al. (1975). Meanders and long waves in the equatorial Atlantic. *Nature*, *257*(5524), 280–284.

ECMWF. (2019). ERA-Interim product [Data set]. Retrieved from https://rda.ucar.edu/datasets/ds627.0/

Flament, P. J., Kennan, S. C., Knox, R. A., Niiler, P. P., & Bernstein, R. L. (1996). The three-dimensional structure of an upper ocean vortex in the tropical Pacific Ocean. *Nature*, *383*(6601), 610–613.

Garzoli, S. (1987). Forced oscillations on the equatorial Atlantic basin during the Seasonal Response of the Equatorial Atlantic Program (1983–1984). *Journal of Geophysical Research: Oceans*, *92*(C5), 5089–5100.

Giordani, H., & Caniaux, G. (2014). Lagrangian sources of frontogenesis in the equatorial Atlantic front. *Climate Dynamics*, *43*, 3147–3162.

Han, W., Liu, W. T., & Lin, J. (2006). Impact of atmospheric submonthly oscillations on sea surface temperature of the tropical Indian Ocean. *Geophysical Research Letters*, *33*(3).

Han, W., Yuan, D., Liu, W. T., & Halkides, D. (2007). Intraseasonal variability of Indian Ocean sea surface temperature during boreal winter: Madden-Julian Oscillation versus submonthly forcing and processes. *Journal of Geophysical Research: Oceans*, *112*(C4).

Hendon, H. H., Liebmann, B., & Glick, J. D. (1998). Oceanic Kelvin waves and the Madden–Julian oscillation. *Journal of the Atmospheric Sciences*, *55*(1), 88–101.

Hoskins, B. J., & Ambrizzi, T. (1993). Rossby wave propagation on a realistic longitudinally varying flow. *Journal of Atmospheric Sciences*, *50*(12), 1661–1671.

Hoskins, B. J., & Karoly, D. J. (1981). The steady linear response of a spherical atmosphere to thermal and orographic forcing. *Journal of the Atmospheric Sciences*, *38*(6), 1179–1196.

Houghton, R. W., & Colin, C. (1987). Wind-driven meridional eddy heat flux in the Gulf of Guinea. *Journal of Geophysical Research: Oceans*, *92*(C10), 10777–10786.

Jochum, M., Malanotte-Rizzoli, P., & Busalacchi, A. (2004). Tropical instability waves in the Atlantic Ocean. *Ocean Modelling*, *7*(1–2), 145–163.

Jouanno, J., Marin, F., du Penhoat, Y., & Molines, J.-M. (2013). Intraseasonal modulation of the surface cooling in the Gulf of Guinea. *Journal of Physical Oceanography*, *43*(2), 382–401.

Karoly, D. J. (1983). Rossby wave propagation in a barotropic atmosphere. *Dynamics of Atmospheres and Oceans*, *7*(2), 111–125.

Kessler, W. S., McPhaden, M. J., & Weickmann, K. M. (1995). Forcing of intraseasonal Kelvin waves in the equatorial Pacific. *Journal of Geophysical Research: Oceans*, *100*(C6), 10613–10631.

Lau, W. K.-M., & Waliser, D. E. (2011). *Intraseasonal variability in the atmosphere-ocean climate system*. Springer Science & Business Media.

Leduc-Leballeur, M., de Coëtlogon, G., & Eymard, L. (2013). Air–sea interaction in the Gulf of Guinea at intraseasonal time-scales: wind bursts and coastal precipitation in boreal spring. *Quarterly Journal of the Royal Meteorological Society*, *139*(671), 387–400.

Legeckis, R. (1977). Long waves in the eastern equatorial Pacific Ocean: A view from a geostationary satellite. *Science*, *197*(4309), 1179–1181.

Li, X., Holland, D. M., Gerber, E. P., & Yoo, C. (2015). Rossby waves mediate impacts of tropical oceans on West Antarctic atmospheric circulation in austral winter. *Journal of Climate*, *28*(20), 8151–8164.

Luther, D. S., & Johnson, E. S. (1990). Eddy energetics in the upper equatorial Pacific during the Hawaii-to-Tahiti Shuttle Experiment. *Journal of Physical Oceanography*, *20*(7), 913–944.

Lyman, J. M., Johnson, G. C., & Kessler, W. S. (2007). Distinct 17-and 33-day tropical instability waves in subsurface observations. *Journal of Physical Oceanography*, *37*(4), 855–872.

Madden, R. A., & Julian, P. R. (1971). Detection of a 40–50 day oscillation in the zonal wind in the tropical Pacific. *Journal of Atmospheric Sciences*, *28*(5), 702–708.

Masina, S., Philander, S., & Bush, A. (1999). An analysis of tropical instability waves in a numerical model of the Pacific Ocean: 2. Generation and energetics of the waves. *Journal of Geophysical Research: Oceans*, *104*(C12), 29637–29661.

McPhaden, M. J., & Taft, B. A. (1988). Dynamics of seasonal and intraseasonal variability in the eastern equatorial Pacific. *Journal of Physical Oceanography*, *18*(11), 1713–1732.

McPhaden, M. J., Busalacchi, A. J., Cheney, R., Donguy, J., Gage, K. S., Halpern, D., et al. (1998). The Tropical Ocean-Global Atmosphere observing system: A decade of progress. *Journal of Geophysical Research: Oceans*, *103*(C7), 14169–14240.

NRL. (2017). GOFS 3.1: 41-layer HYCOM + NCODA Global 1/12° Reanalysis [Data set]. Retrieved from https://www.hycom.org/dataserver/gofs-3pt1/reanalysis

Patricola, C. M., & Chang, P. (2017). Structure and dynamics of the Benguela low-level coastal jet. *Climate Dynamics*, *49*(7), 2765–2788.

Philander, S. (1976). Instabilities of zonal equatorial currents. *Journal of Geophysical Research*, *81*(21), 3725–3735.

Philander, S. (1978). Instabilities of zonal equatorial currents, 2. *Journal of Geophysical Research: Oceans*, *83*(C7), 3679–3682.

Proehl, J. A. (1996). Linear stability of equatorial zonal flows. *Journal of Physical Oceanography*, *26*(4), 601–621.

Remote Sensing Systems. (2022). Cross-Calibrated Multi-Platform (CCMP) Ocean Winds V3.0 [Data set]. Retrieved from https://data.remss.com/ccmp/v03.0/daily/

Reynolds, R. W., Smith, T. M., Liu, C., Chelton, D. B., Casey, K. S., & Schlax, M. G. (2007). Daily high-resolution-blended analyses for sea surface temperature. *Journal of Climate*, *20*(22), 5473–5496.

Reynolds, R. W., Smith, T. M., Liu, C., Chelton, D. B., Casey, K. S., Schlax, M. G., & Huang, B. (2007). NOAA OI SST V2 High Resolution Dataset [Data set]. Retrieved from https://psl.noaa.gov/data/gridded/data.noaa.oisst.v2.highres.html

Risien, C. M., Reason, C., Shillington, F., & Chelton, D. B. (2004). Variability in satellite winds over the Benguela upwelling system during 1999–2000. *Journal of Geophysical Research: Oceans*, *109*(C3).

Shimizu, M. H., & de Albuquerque Cavalcanti, I. F. (2011). Variability patterns of Rossby wave source. *Climate Dynamics*, *37*, 441–454.

Shinoda, T., Hendon, H. H., & Glick, J. (1998). Intraseasonal variability of surface fluxes and sea surface temperature in the tropical western Pacific and Indian Oceans. *Journal of Climate*, *11*(7), 1685–1702.

Torrence, C., & Compo, G. P. (1998). A practical guide to wavelet analysis. *Bulletin of the American Meteorological Society*, *79*(1), 61–78.

Von Schuckmann, K., Brandt, P., & Eden, C. (2008). Generation of tropical instability waves in the Atlantic Ocean. *Journal of Geophysical Research: Oceans*, *113*(C8).

Wyrtki, K. (1981). An estimate of equatorial upwelling in the Pacific. *Journal of Physical Oceanography*, *11*(9), 1205–1214.

Xie, S.-P., & Carton, J. A. (2004). Tropical Atlantic variability: Patterns, mechanisms, and impacts. *Earth's Climate: The Ocean-Atmosphere Interaction, Geophys. Monogr*, *147*, 121–142.

Yu, J., & Liu, W. T. (2003). A linear relationship between ENSO intensity and tropical instability wave activity in the eastern Pacific Ocean. *Geophysical Research Letters*, *30*(14).